NASA/TP—2008-214943 ARL–TR–4200

Heat Transfer in a Superelliptic Transition Duct

Philip Poinsatte
Glenn Research Center, Cleveland, Ohio

Douglas Thurman
U.S. Army Research Laboratory, Glenn Research Center, Cleveland, Ohio

Steven Hippensteele
Glenn Research Center, Cleveland, Ohio

May 2008

NASA STI Program . . . in Profile

Since its founding, NASA has been dedicated to the advancement of aeronautics and space science. The NASA Scientific and Technical Information (STI) program plays a key part in helping NASA maintain this important role.

The NASA STI Program operates under the auspices of the Agency Chief Information Officer. It collects, organizes, provides for archiving, and disseminates NASA's STI. The NASA STI program provides access to the NASA Aeronautics and Space Database and its public interface, the NASA Technical Reports Server, thus providing one of the largest collections of aeronautical and space science STI in the world. Results are published in both non-NASA channels and by NASA in the NASA STI Report Series, which includes the following report types:

- TECHNICAL PUBLICATION. Reports of completed research or a major significant phase of research that present the results of NASA programs and include extensive data or theoretical analysis. Includes compilations of significant scientific and technical data and information deemed to be of continuing reference value. NASA counterpart of peer-reviewed formal professional papers but has less stringent limitations on manuscript length and extent of graphic presentations.

- TECHNICAL MEMORANDUM. Scientific and technical findings that are preliminary or of specialized interest, e.g., quick release reports, working papers, and bibliographies that contain minimal annotation. Does not contain extensive analysis.

- CONTRACTOR REPORT. Scientific and technical findings by NASA-sponsored contractors and grantees.

- CONFERENCE PUBLICATION. Collected papers from scientific and technical conferences, symposia, seminars, or other meetings sponsored or cosponsored by NASA.

- SPECIAL PUBLICATION. Scientific, technical, or historical information from NASA programs, projects, and missions, often concerned with subjects having substantial public interest.

- TECHNICAL TRANSLATION. English-language translations of foreign scientific and technical material pertinent to NASA's mission.

Specialized services also include creating custom thesauri, building customized databases, organizing and publishing research results.

For more information about the NASA STI program, see the following:

- Access the NASA STI program home page at *http://www.sti.nasa.gov*

- E-mail your question via the Internet to *help@sti.nasa.gov*

- Fax your question to the NASA STI Help Desk at 301–621–0134

- Telephone the NASA STI Help Desk at 301–621–0390

- Write to:
  NASA Center for AeroSpace Information (CASI)
  7115 Standard Drive
  Hanover, MD 21076–1320

NASA/TP—2008-214943 ARL–TR–4200

Heat Transfer in a Superelliptic Transition Duct

Philip Poinsatte
Glenn Research Center, Cleveland, Ohio

Douglas Thurman
U.S. Army Research Laboratory, Glenn Research Center, Cleveland, Ohio

Steven Hippensteele
Glenn Research Center, Cleveland, Ohio

National Aeronautics and
Space Administration

Glenn Research Center
Cleveland, Ohio 44135

May 2008

This work was sponsored by the Fundamental Aeronautics Program
at the NASA Glenn Research Center.

Level of Review: This material has been technically reviewed by expert reviewers.

Available from

NASA Center for Aerospace Information
7115 Standard Drive
Hanover, MD 21076–1320

National Technical Information Service
5285 Port Royal Road
Springfield, VA 22161

Available electronically at http://gltrs.grc.nasa.gov

Heat Transfer in a Superelliptic Transition Duct

Philip Poinsatte
National Aeronautics and Space Administration
Glenn Research Center
Cleveland, Ohio 44135

Douglas Thurman
National Aeronautics and Space Administration
U.S. Army Research Laboratory
Cleveland, Ohio 44135

Steven Hippensteele
National Aeronautics and Space Administration
Glenn Research Center
Cleveland, Ohio 44135

Summary

Local heat transfer measurements were experimentally mapped using a transient liquid-crystal heat transfer technique on the surface of a circular-to-rectangular transition duct. The transition duct had a length-to-diameter ratio of 1.5 and an exit-plane aspect ratio of 3. The cross-sectional geometry was defined by the equation of a superellipse. The cross-sectional area was the same at the inlet and exit but varied up to 15 percent higher through the transition.

The duct was preheated to a uniform temperature (nominally 64 °C) before allowing room temperature air to be suddenly drawn through it. As the surface cooled, the resulting isothermal contours on the duct surface were revealed using a surface coating of thermochromic liquid crystals that display distinctive colors at particular temperatures. A video record was made of the surface temperature and time data for all points on the duct surfaces during each test. Using this surface temperature-time data together with the temperature of the air flowing through the model and the initial temperature of the model wall, the heat transfer coefficient was calculated by employing the classic one-dimensional, semi-infinite wall heat transfer conduction model.

Test results are reported for inlet diameter-based Reynolds numbers ranging from 0.4×10^6 to 2.4×10^6 and two grid-generated freestream turbulence intensities of about 1 percent, which is typical of wind tunnels, and up to 16 percent, which may be more typical of real engine conditions.

Introduction

Recent designs of engine exhaust ducts and nozzles for military aircraft have often moved away from round exits to the more advanced rectangular or irregular-shaped exits. These newly designed exits have two main areas of benefit: lower observable infrared signatures from nozzles and increased performance through vectoring of exhaust nozzles. In a jet engine the new designs require a transition duct going from the round cross section turbine exit to the rectangular cross section nozzle.

Additionally, as part of the continuing effort to increase overall gas-turbine efficiency, higher engine operating temperatures and pressures can be used. Employing higher gas temperatures and pressures increases the importance of knowing the temperatures on the gas path surfaces. More complex cooling configurations may be needed to provide acceptable metal temperatures and component life. The attainment of accurate metal temperature predictions to ensure effectively cooled and durable parts requires accurate knowledge of high-resolution heat transfer coefficients.

The changing of exhaust flow path geometry coupled with efforts to increase engine operating temperature leads to concerns about items such as drag and metal surface temperature. A generic superelliptic duct with a round inlet and rectangular exit was designed to measure fluid mechanics and heat transfer by the NASA Glenn Research Center. Extensive aerodynamic data on this superelliptic duct was obtained by Davis (ref. 1) and Reichert (ref. 2). The design and development history of this duct and previous work is detailed in those references. The same duct geometry was used in the current study to measure surface heat transfer. Experimental work continued in this area, including the addition of swirl to transition duct flow (ref. 3). Computational efforts by Cavicchi (ref. 4), Harloff et al. (ref. 5), Sotiropoulos and Patel (ref. 6), and Wang et al. (ref. 7) have examined the flow characteristics of circular to rectangular ducts. Heat transfer measurements and computations have been made on a square to rectangular duct (ref. 8). The present work adds the surface heat transfer distribution to the round-to-rectangular superelliptic duct benchmark database. A list of symbols found in this report is given in appendix A.

Description of Technique

Theory

Heat transfer coefficients for this study were determined by using a transient method in which a heated duct wall surface is rapidly cooled with room temperature air. Thermochromic liquid crystals were sprayed on the surface of the duct model

and were used to unobtrusively indicate resulting surface temperatures as the airflow cooled the surface.

This method (refs. 9 and 10) assumes that the penetration depth of the cooling pulse into the duct wall is small compared to the wall thickness or local radius of curvature. Therefore, the heat conduction out of the duct wall may be considered to be one-dimensional out of a semi-infinite medium and can be described by the equation

$$\frac{\partial^2 T}{\partial s^2} = \frac{1}{\alpha}\frac{\partial T}{\partial t} \tag{1}$$

where T is temperature, s is distance into the duct wall surface, α is thermal diffusivity, and t is time. The heat flux q at the surface is

$$q = h(T_s - T_r) = -\left.\frac{k_w \partial T}{\partial s}\right|_{s=0} \tag{2}$$

where h is the heat transfer coefficient, T_s is the duct wall surface temperature as shown by the liquid crystals, T_r is the air recovery temperature (see eq. (6)), and k_w is the duct wall thermal conductivity. This equation may be solved for a step function of flow to give the nondimensional surface temperature as a function of nondimensional time through the complimentary error function as follows:

$$\theta = 1 - e^{\beta^2}\,\mathrm{erfc}(\beta) \tag{3}$$

Here, θ and β are the nondimensional temperature and time, respectively, defined as

$$\theta = \frac{T_i - T_s}{T_i - T_r} \tag{4}$$

$$\beta = \frac{h\sqrt{t}}{\sqrt{\rho c k_w}} \tag{5}$$

where T_i is the initial surface temperature, ρ is the density of the duct wall material, and c is the specific heat of the duct wall material. Note that h and T_r in the above equations are assumed constant over the duration of the test.

Hence it can be seen that if the duct wall thermal properties (ρ, c, and k_w), air temperature (T_r), and initial duct wall surface temperature (T_i) are known, then the heat transfer coefficients h can be found at the duct wall for a given surface temperature T_s and time from airflow startup t. By using microencapsulated and noninteracting thermochromic liquid crystals sprayed onto the duct surface to indicate the surface temperature at various times, one can obtain a quantitative surface map for h. This is the principle of the transient method utilizing liquid crystals for calculating surface heat transfer coefficients.

For the present work, the duct wall material was chosen to be acrylic, which has suitable thermal properties as well as having clarity for visibility. It should be noted that in order to avoid violating the semi-infinite wall assumption, the heat conduction penetration depth must not be exceeded. The acrylic walls were 0.5 in. thick, thus allowing a penetration time of about 2 min. The surface temperature can be determined from the color bands that are formed by the liquid crystal paint, which correspond to specific temperatures. For the current study, a narrow-band liquid crystal ~1 °C (2 °F) wide was used, with the yellow color showing an isotherm corresponding to a calibrated temperature of 38.2 °C (101 °F). Narrow-band crystals have the advantage of being less susceptible to camera-to-light angle refraction effects and, in the present case with a well defined test, essentially render these effects negligible. During a test run, the liquid crystal patterns that are formed as the surface is cooled are recorded using color video cameras and video recorders. Video images were digitized at specific time intervals with a color frame grabber. The yellow isotherms at each time interval were extracted from the digitized video image. If more than one camera view was used, the isotherm data from the various views were combined into a composite file and converted into surface coordinates.

The inlet recovery temperature T_r was determined from the measured inlet total temperature T_{to} and calculated inlet static temperature T_{st}:

$$T_r = T_{st} + r(T_{to} - T_{st}) \tag{6}$$

A turbulent boundary layer was assumed, and thus a value of 0.892 was calculated for the recovery factor r. An average value of T_{to} was obtained by integrating the temperature from startup of the tunnel air to the time of the particular video frame.

Once the above temperatures were known, the nondimensional temperature θ could be calculated from equation (4) at any location on the surface of the duct wall. Additionally, the nondimensional time β, for a specific θ, could be calculated from equation (3). Finally, using equation (5), for a specific time t, the heat transfer coefficient h could be calculated at the particular surface location where the yellow-colored isotherm lies. Since this duct was tested at a relatively low Mach number and the velocity did not vary significantly through the duct, the local recovery temperature was considered to be constant over the entire duct floor and equal to that at the inlet of the duct. This also meant that the liquid crystal isotherm had a constant heat transfer coefficient value along its entire length. This may not be true when local velocities vary greatly, either in other types of models or in cases having high Mach numbers. A varying local recovery temperature would result in liquid crystal isotherms having different heat transfer coefficients along their lengths and would require appropriate adjustment of data reduction.

The heat transfer coefficient was made dimensionless by calculating the Nusselt number as follows:

$$\mathrm{Nu} = \frac{hD}{k_a} \tag{7}$$

where D is the duct inlet diameter and k_a is the thermal conductivity of air.

Finally, the Nusselt numbers were normalized by the values for turbulent flow in a circular tube:

$$Nu_0 = 0.023\left(Re^{0.8}\right)\left(Pr^{0.4}\right) \quad (8)$$

where Re is the Reynolds number based on inlet diameter and Pr is the Prandtl number for room temperature air.

Apparatus

Facility

The Transition Duct Heat Transfer Tunnel in the Engine Research Building (ERB), SW–2, at the NASA Glenn Research Center is shown in figures 1 and 2. Altitude exhaust vacuum drew room temperature air through the wind tunnel which consisted of an inlet bellmouth, flow conditioning screens and honeycomb, a 12:1 area contraction section, a roughly 2-diameter-long straight spool section, a probe section, and the superelliptic transition duct being tested. The air then passed through a straight downstream section, an exit adapter section, a fast-opening 30.5-cm (12-in.) round valve, a flow-control valve, and into the central altitude exhaust system. A 2.54-cm (1-in.) band of coarse grit sandpaper was attached to the tunnel wall at the end of the contraction section to ensure turbulent boundary layer flow and to match the trip used by Davis (ref. 1). For some test cases, a high-turbulence-generating grid was installed approximately 1 diameter upstream of the test section. The grid was constructed of 1.27-cm (0.5-in.) horizontal and vertical square bars with 5.08-cm (2-in.) centerline spacing. The cross section blockage due to the grid was approximately 43 percent.

Cameras were placed to view the top and side of the test section. Low-heat-emitting lights were used to illuminate the model. A microswitch on the fast valve activated a video timer superimposed on the video signal from each camera as well as a light-emitting diode placed in the video camera field of view, which indicated when the airflow started. This microswitch also produced an electrical signal that was recorded by the data acquisition system to indicate the airflow start time.

Figure 1.—NASA Glenn Engine Research Building SW–2 Transition Duct Heat Transfer Tunnel.

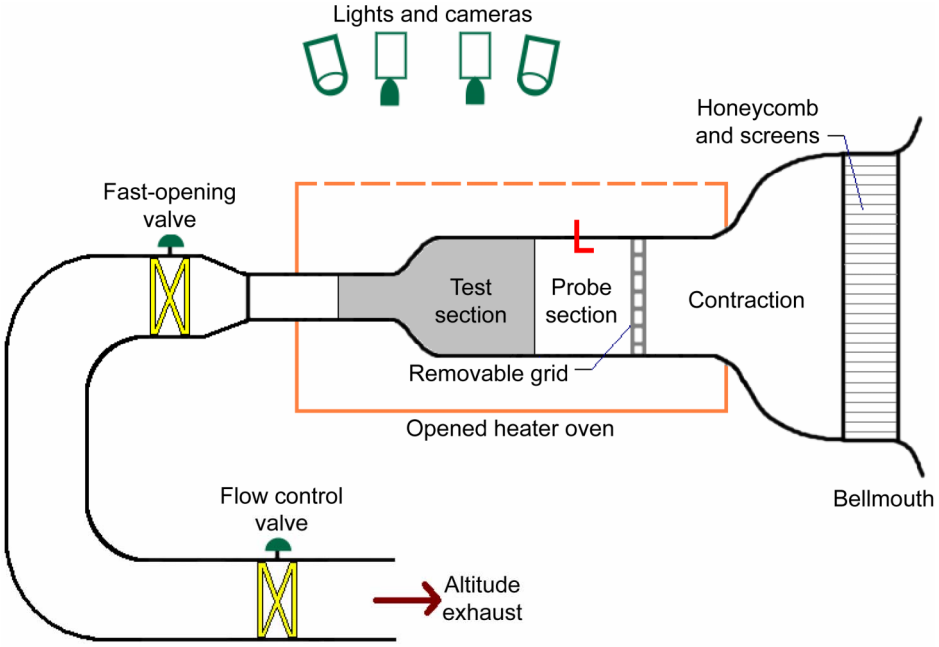

Figure 2.—Transition Duct Heat Transfer Tunnel (not to scale).

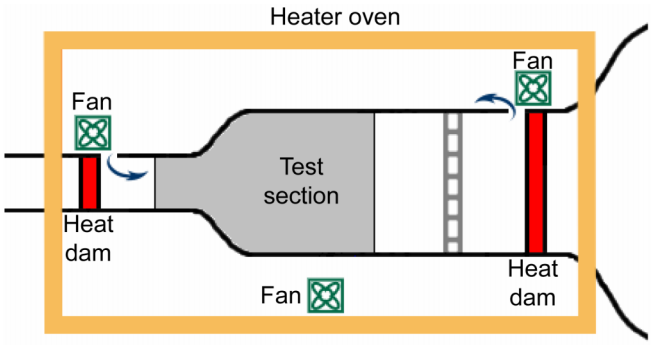

Figure 3.—Heater oven detail (see fig. 2) in Transition Duct Heat Transfer Tunnel.

Prior to the test, the duct surfaces were uniformly heated using the heating system shown in figure 3. A heater oven using automatic temperature-controlled electric heater blankets surrounded the test model. An internal hot air loop through the inside of the test duct was established using two removable insulated heat dams located at the inlet and exit ends of the test duct and several circulating fans. The fans circulated the hot air through the duct and through the oven. This allowed the nonuniformity of the temperature of the test duct model wall to be held very small. Temperature and pressure measurements were recorded on an automated data acquisition system at roughly 15 Hz. Surface transient temperatures were determined from the liquid crystal calibrated colors. Video images were acquired by RGB (red-green-blue) video cameras and recorded on Betacam SP (Sony Corporation) videotape.

The inlet airflow conditions were as follows: room temperature air, nominally 21 °C (70 °F); atmospheric pressure, nominally 98.5 kPa (14.3 psia); flow rates between 1.2 and 7.1 kg/s (2.7 and 15.6 lbm/s); velocities between 27.4 and 181.4 m/s (90 and 595 ft/s); Mach numbers between 0.08 and 0.55; Prandtl number nominally 0.71; and inlet Reynolds numbers based on the duct inlet diameter between 0.40×10^6 and 2.40×10^6.

Test model

The superelliptic transition duct test section was made of acrylic and is shown in figure 4. Its cross-sectional shape was described by a superelliptical equation with varying coefficients listed in table I. The duct had a circular inlet with a diameter of 22.225 cm (8.75 in.) and a 3:1 nearly rectangular exit of 34.5 cm (13.5 in.) wide by 11.5 cm (4.5 in.) high. Its overall length was 77.8 cm (30.625 in.), or 3.5 diameters. The transition from circular to rectangular cross section took place between $x/D = 1$ and $x/D = 2.5$. The duct inlet and exit had the same cross-sectional area of roughly 390 cm^2 (60 $in.^2$). The cross-sectional area gradually diverged about 15 percent at roughly $x/D = 1.75$, then converged back to a value equal to that of the inlet.

This slightly varying area caused the air velocity to decrease then increase as it passed through the duct. The transition duct then flowed into a 0.6-m (2-ft) long, constant-cross-section exit.

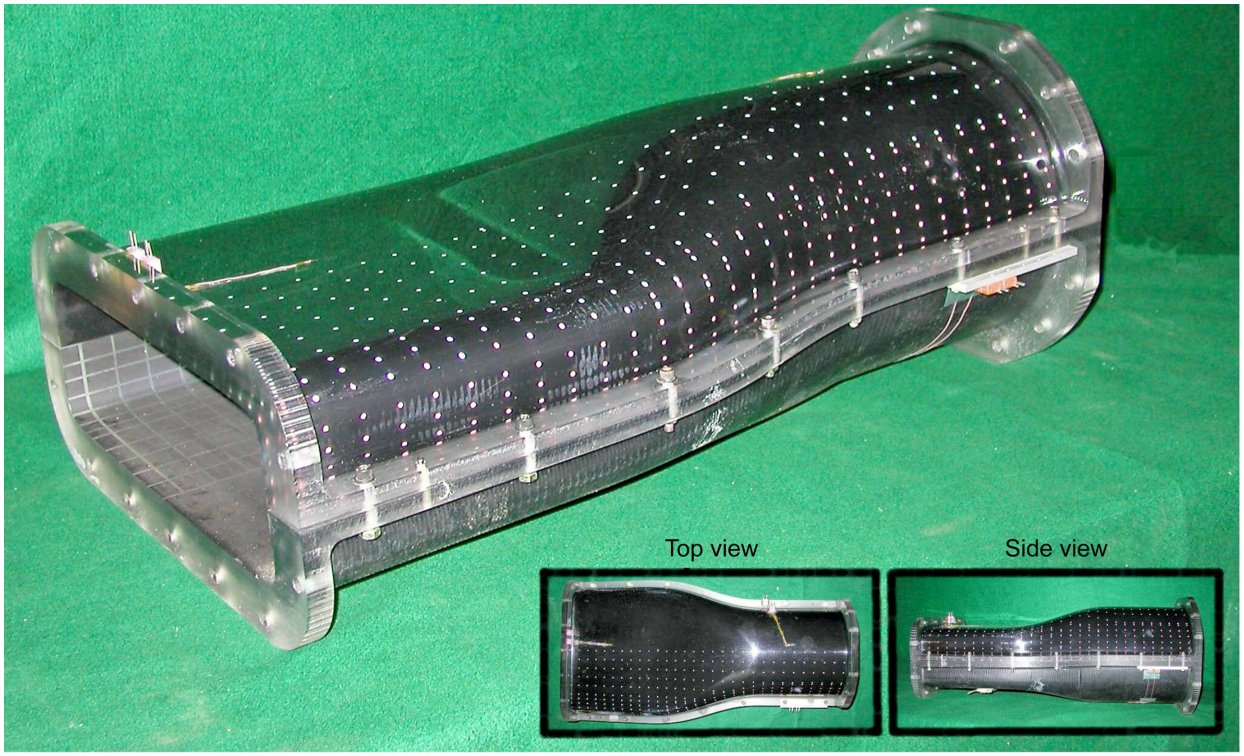

Figure 4.—Superelliptic transition duct test section.

TABLE I.—TRANSITION DUCT GEOMETRY VARIABLES[a]
[$(y/a)^n + (z/b)^n = 1$ and $R = 4.375$ in.]

Normalized coordinate, x/R	Normalized geometry coefficient, a/R	Normalized geometry coefficient, b/R	Geometry exponent, n	Aspect ratio	Normalized cross-sectional area
0.00	1.0000	1.0000	2.0000	1.0000	1.0000
2.00	1.0000	1.0000	2.0000	1.0000	1.0000
2.12	1.0003	.9997	2.1047	1.0006	1.0192
2.24	1.0025	.9978	2.2151	1.0047	1.0376
2.36	1.0078	0.9831	2.3331	1.0251	1.0555
2.48	1.0174	.9746	2.4588	1.0439	1.0729
2.60	1.0316	.9719	2.5934	1.0614	1.0897
2.72	1.0509	.9548	2.7383	1.1006	1.1056
2.84	1.0752	0.9333	2.8947	1.1520	1.1198
2.96	1.1041	.9177	3.0645	1.2031	1.1319
3.08	1.1371	.8784	3.2497	1.2945	1.1410
3.20	1.1734	.8462	3.4528	1.3867	1.1464
3.32	1.2123	0.8117	3.6770	1.4935	1.1475
3.44	1.2527	.7759	3.9261	1.6145	1.1441
3.56	1.2936	.7396	4.2050	1.7491	1.1362
3.68	1.3341	.7037	4.5199	1.8958	1.1241
3.80	1.3729	0.6693	4.8791	2.0512	1.1087
3.92	1.4093	.6370	5.2932	2.2124	1.0911
4.04	1.4423	.6078	5.7775	2.3730	1.0725
4.16	1.4712	.5821	6.3524	2.5274	1.0544
4.28	1.4954	0.5606	7.0484	2.6675	1.0381
4.40	1.5147	.5435	7.9106	2.7869	1.0248
4.52	1.5290	.5308	9.0131	2.8806	1.0152
4.64	1.5385	.5224	10.000	2.9451	1.0083
4.76	1.5439	0.5176	10.000	2.9828	1.0026
4.88	1.5460	.5157	10.000	2.9979	1.0003
5.00	1.5464	.5154	10.000	3.0000	1.0000
7.00	1.5464	.5154	10.000	3.0000	1.0000

[a]Coordinate system is illustrated in figure 5.

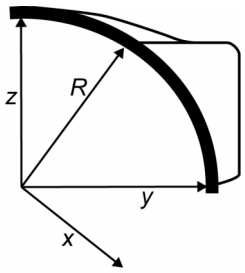

Figure 5.—Duct coordinate system.

The transition duct model had two overlapping grids marked on one quadrant, one a top view normal projection and the other a side view normal projection. The grid intersection points were digitized from reference video frames and used to interpolate the position of the yellow-colored isotherms on the data video frames. During each test run, the duct was videotaped with two cameras as the surface changed temperature. At specific time intervals, video images from the two views were digitized with a color frame grabber. Isotherms at each interval were extracted from the digitized video images, and their projected view positions were determined with use of the projected view grid files. The isotherm data from the various views were then put into a composite file and transformed back to the surface coordinates.

The transient technique that was employed for measuring duct surface temperatures used thermochromic liquid crystals that were painted onto the test duct floor. The thermochromic liquid crystals were a microencapsulated, chiral-nematic, narrow-band (~1 °C (2 °F)) type manufactured by Halcrest, Incorporated. The liquid crystal slurry from the manufacturer was diluted and mixed with an acylic binder and air sprayed onto the surface. These crystals have the property of changing color with temperature and were calibrated on that property. A change in the angle between incident light and camera view will cause a refractive shift in visible color observed and may alter the color-temperature calibration of the liquid crystal. Using narrow-band crystals lessens this problem drastically: the narrow band yields a small temperature variation with the changing angle even with a relatively large refractive color shift. Keeping the light-to-camera angles fairly small and employing narrow band liquid crystals essentially eliminates this calibration concern.

Prior to testing, the test model was heated to a uniform and constant temperature, in some cases as high as 71 °C (159 °F). After reaching this steady uniform thermal condition the model was suddenly cooled with room-temperature airflow. The test section was illuminated with low-heat-emitting lighting so the temperature of the liquid-crystal-coated test surface was not altered. The duct surface temperatures were measured by type E thin-film thermocouples attached to the inside and outside of the model. These thermocouples were used to determine the initial surface temperature and were also used in liquid crystal color calibration. The airstream velocity was determined by total and static pressure difference measured by pressure transducers.

Procedure

Inlet surveys

Radial pressure surveys were obtained using actuator-driven pitot and boundary layer pressure probes at a location upstream of the duct test section. Steady-state probe pressures were measured with strain-gage-type transducers and an analog-to-digital data system. Measurements were made at several circumferential positions at various tunnel flow conditions. Additionally, turbulence measurements were acquired at the same upstream location using commercial hot wire equipment.

Heat transfer measurements

Prior to commencing the airflow, the acrylic duct wall surface was heated to a prescribed temperature that would ensure surface cooling through the liquid crystal temperature color range within the penetration time. The duct was preheated in the surrounding oven to the required temperature, which ranged from 58 to 71 °C (136 to 159 °F). By waiting a few hours the temperature nonuniformity of the test duct model wall was held to within a few tenths of a degree Fahrenheit. This initial temperature was measured at various places on the duct wall on both the inside and outside surfaces. The median value of the initial surface temperatures was taken for each test run as a constant value, and a maximum deviation among the surface temperatures was used in the uncertainty analysis (see appendix B).

The main airflow-control valve in the altitude (vacuum) exhaust pipe located downstream was set to produce the desired Reynolds number flow. Once an equilibrium temperature was reached on the model, the heat dams were replaced with the tunnel covers, and the video and data recording devices were started. The fast valve was then opened (in less than 0.067 s) to suddenly start the airflow to cool the duct with the room temperature air. After the test run of no longer than 2 min was completed, the fast-opening valve was closed, and the model was preheated for the next test.

The surface temperature T_s was determined from the calibrated yellow liquid crystal color. The yellow-band isotherms having calibrated temperatures of 38.2 °C (101 °F) were recorded as a function of time using the two RGB video cameras and Betacam SP video recorders. The cameras were positioned such that one viewed the upstream half of the duct and the other viewed the downstream section.

Video processing

The heat transfer data reduction was done using a personal computer equipped with a commercial video frame grabbing board employing a hue, saturation, intensity (HSI) color definition. An automatic color extraction method had been developed (refs. 11 and 12) using hue values to recover isotherms from video frames. The current technique used not only a specified hue value range to extract the yellow color but also employed various combinations of saturation and intensity thresholds. This aided in alleviating many difficulties associated with glares and uneven lighting that are common in videotaping real-world test models with compound curved surfaces. In some flow situations the isotherm details still could not always be obtained automatically, especially in regions with high temperature gradients. Therefore, as well as autodigitizing, the computer program allowed manual digitizing (tracing) of the yellow color bands from a video image grabbed from the video tape. The image was digitized and stored in a computer file. Another program then corrected for skewed views, which may occur when viewing the test area at an angle other than 90° or when the view was distorted by looking at or through a curved acrylic model wall. This was accomplished using the projected view grid files along with the projected view isotherm files. The isotherm locations were linearly interpolated between the appropriate grid points and then transformed back to surface coordinates. The digitized locations of the yellow-band surface isotherms along with the measurements of times and the initial temperatures from the online data acquisition system allowed for the calculation of heat transfer coefficients.

Results and Discussion

Inlet Pressure Surveys

Inlet flow surveys were measured using a total pressure probe and a boundary layer probe. Measurements were taken at the probe section just upstream of the duct inlet. Typical results of mean velocity profiles and law of wall profiles are shown in figures 6 and 7, respectively, and are generally consistent with turbulent flow profiles. Table II summarizes calculated boundary layer thickness, displacement thickness, momentum thickness and shape factor as a function of Mach number. The shape factor generally matches Davis (ref. 1) and Reichert (ref. 2) data within 7 percent and is typical of turbulent pipe flow.

Turbulence

Turbulence measurements were made using a commercial hot wire system. In the open tunnel cases (no grid), the measured turbulence intensities for various Reynolds numbers were nominally 1 percent. For the cases with the turbulence-generating grid installed, the turbulence intensities were measured to be around 16 percent at a location roughly 1 diameter downstream of the grid. This turbulence matched values from the Baines and Peterson correlation (ref. 13) and was expected to decay with distance according to the correlation.

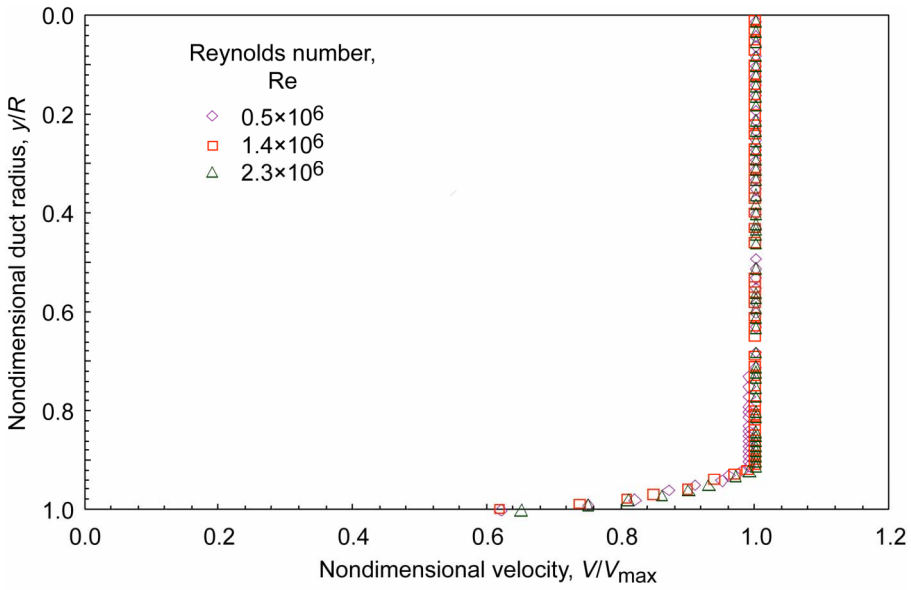

Figure 6.—Superelliptic transition duct inlet velocity profile at three Reynolds numbers.

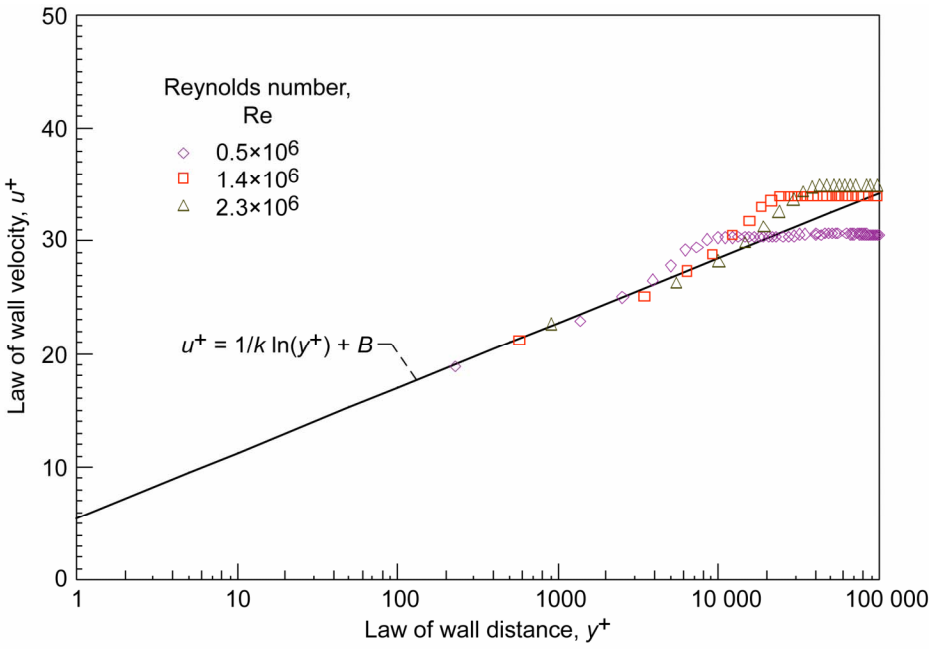

Figure 7.—Superelliptic transition duct inlet velocity profile at three Reynolds numbers.

TABLE II.—TRANSITION DUCT BOUNDARY LAYER PARAMETERS

Mach number, M	Reynolds number, Re	Boundary layer thickness,[a] $\delta_{.95}/R$	Displacement thickness,[a] δ^*/R	Momentum thickness,[a] θ_m/R	Shape factor,[b] H
0.10	0.50×10^6	0.060	0.0116	0.0089	1.30
.30	1.40	.065	.0114	.0085	1.34
.55	2.30	.060	.0112	.0086	1.30

[a]Radius R = 11.11 cm (4.375 in.).
[b]$H = \delta^*/\theta_m$.

Heat Transfer

Heat transfer measurements were made for high- and low-turbulence cases at three Reynolds numbers each. Heat transfer coefficients were based on the inlet velocity and calculated using equations (3) through (6). Results are presented as Nusselt number, calculated from equation (7). Heat transfer run conditions are summarized in table III. Uncertainties in heat transfer coefficients, as described in appendix B, were nominally 5 percent. Note all heat transfer data are available either online or on CD. The Uniform Resource Locators (URLs) for these files are found at the end of this report on the Report Documentation Page under "Supplementary Notes."

Figure 8 shows surface heat transfer contours for the cases with low turbulence and Reynolds numbers of 0.4×10^6, 1.6×10^6, and 2.4×10^6. Note that the figure shows data for one quadrant only. The heat transfer pattern for the three cases is similar. Note that "holes" in the contours are the result of lighting glares in the video frames, which obstructed the data acquisition in these regions. For the lowest Reynolds number case (fig. 8(a)), Nusselt numbers range from 260 to 690, with the maximum Nusselt number being 2.65 times larger than the minimum Nusselt number. Similarly for the middle Reynolds number case (fig. 8(b)), the Nusselt number varies from 750 to 2050, and the high Nusselt number is 2.73 times larger than the low Nusselt number. Finally, the Nusselt number for the high Reynolds number case (fig. 8(c)) varies from 1000 to 3000, and the high Nusselt number is 3.0 times larger than the low value. The highest heat transfer is caused by the impingement of airflow at the point where the round duct flattens out on the top surface. The heat transfer gradually decreases outward from this maximum. The lowest heat transfer is seen where the pressure gradient decreases as the duct fans out on the sides. As the duct flattens on the top and bottom and spreads out on the sides, a pattern of counterrotating vortices is set up on each side of the duct (see refs. 1 and 2). These vortex flows result in the surface heat transfer patterns of streaks of local maximums and minimums seen on the downstream rectangular section of the duct. Based on maximum and minimum values, Nusselt number generally increases with Reynolds number to the 0.8 power. A local maximum near the entrance of the duct is also present.

Figure 9 shows surface heat transfer for the cases with high turbulence and Reynolds numbers of 0.40×10^6, 0.77×10^6, and 1.40×10^6. Compared with the low-turbulence cases, the general shape of the heat transfer pattern has not changed except near the inlet of the duct where the higher turbulence has caused an increase in the heat transfer. The high heat transfer at the inlet drops fairly quickly; this is most likely due to relatively rapid decay of the grid-induced turbulence. The heat transfer in the downstream section seems to be less smooth and perhaps the flow less stable relative to the low turbulence cases. Figures 8(a) and 9(a) allow a direct comparison for the effect of turbulence intensity on heat transfer, as the Reynolds numbers are constant for both cases. The higher turbulence causes a reduction in the range of measured heat transfer values for each particular case. Figure 9(a) shows the results for the Reynolds number of 0.40×10^6: the Nusselt numbers range from a low of 440 to a high value of 740 with the high number being 1.68 times larger than the low number. Figure 9(b) shows the results for the Reynolds number of 0.77×10^6: the Nusselt numbers range from 800 to 1350, and the high Nusselt number is 1.69 times larger than the lower number. Likewise, figure 9(c) shows the results for the Reynolds number of 1.40×10^6: the heat transfer ranges from 1300 to 2550, with the high Nusselt number 1.96 times larger than the lower.

TABLE III.—TRANSITION DUCT HEAT TRANSFER TEST CONDITIONS

Inlet velocity, V, m/s	Mach number, M	Reynolds number, Re	Initial temperature, T_i, °C	Nominal recovery temperature, T_r, °C	Liquid crystal temperature, T_{lc}, °C	Turbulence intensity, Tu, percent
29	0.08	0.40×10^6	58	21	38.2	1
114	.34	1.60	67	19	38.2	1
181	.55	2.40	71	18	38.2	1
27	.08	.40	58	21	38.2	16
56	.16	.77	62	20	38.2	16
165	.49	1.40	68	18	38.2	16

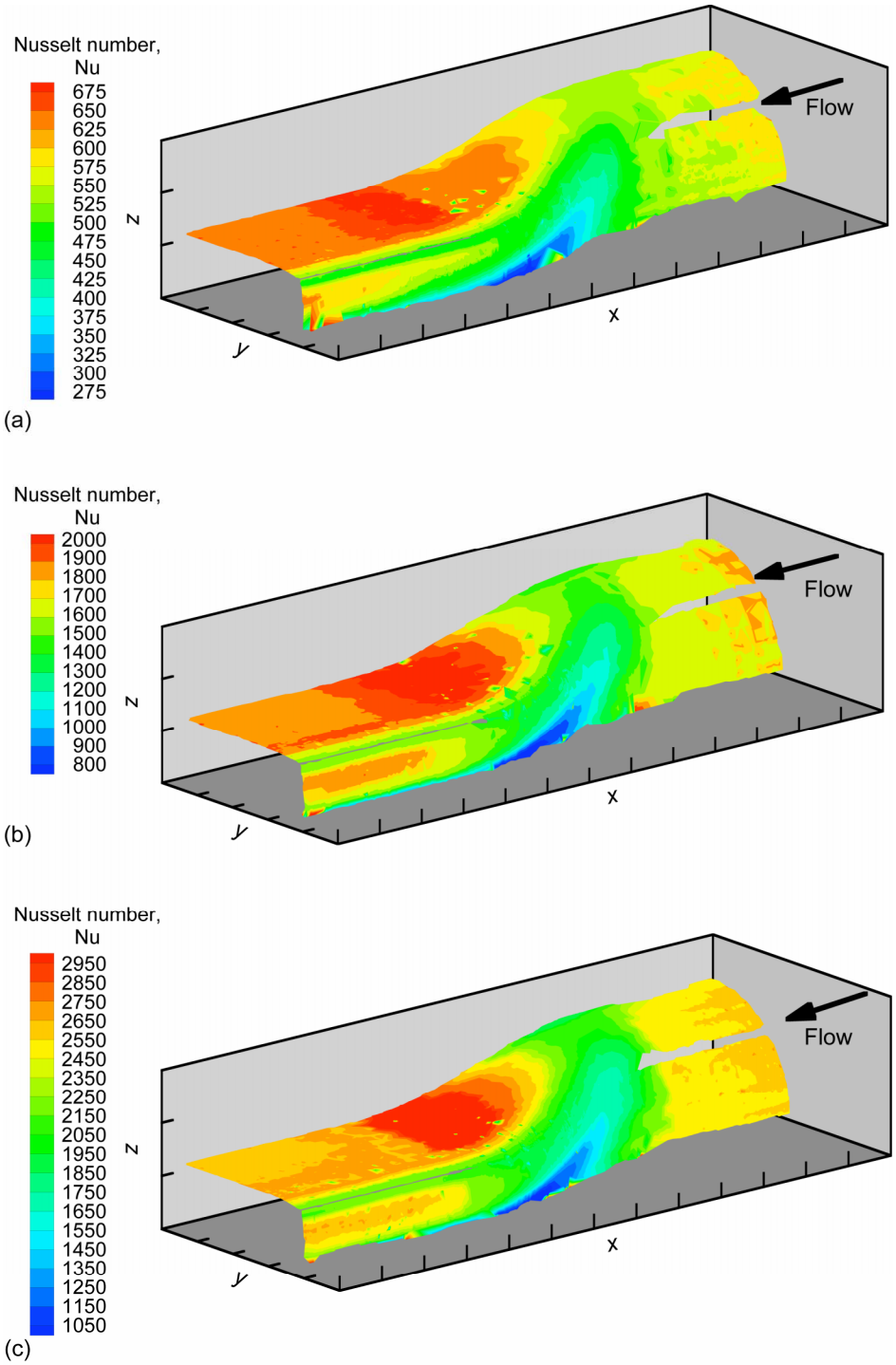

Figure 8.—Heat transfer contours at nominal 1 percent turbulence intensity (*Tu*) at three Reynolds numbers (Re) and Mach numbers (M). (a) Re = 0.4×10^6 and M = 0.08. (b) Re = 1.6×10^6 and M = 0.34. (c) Re = 2.4×10^6 and M = 0.55.

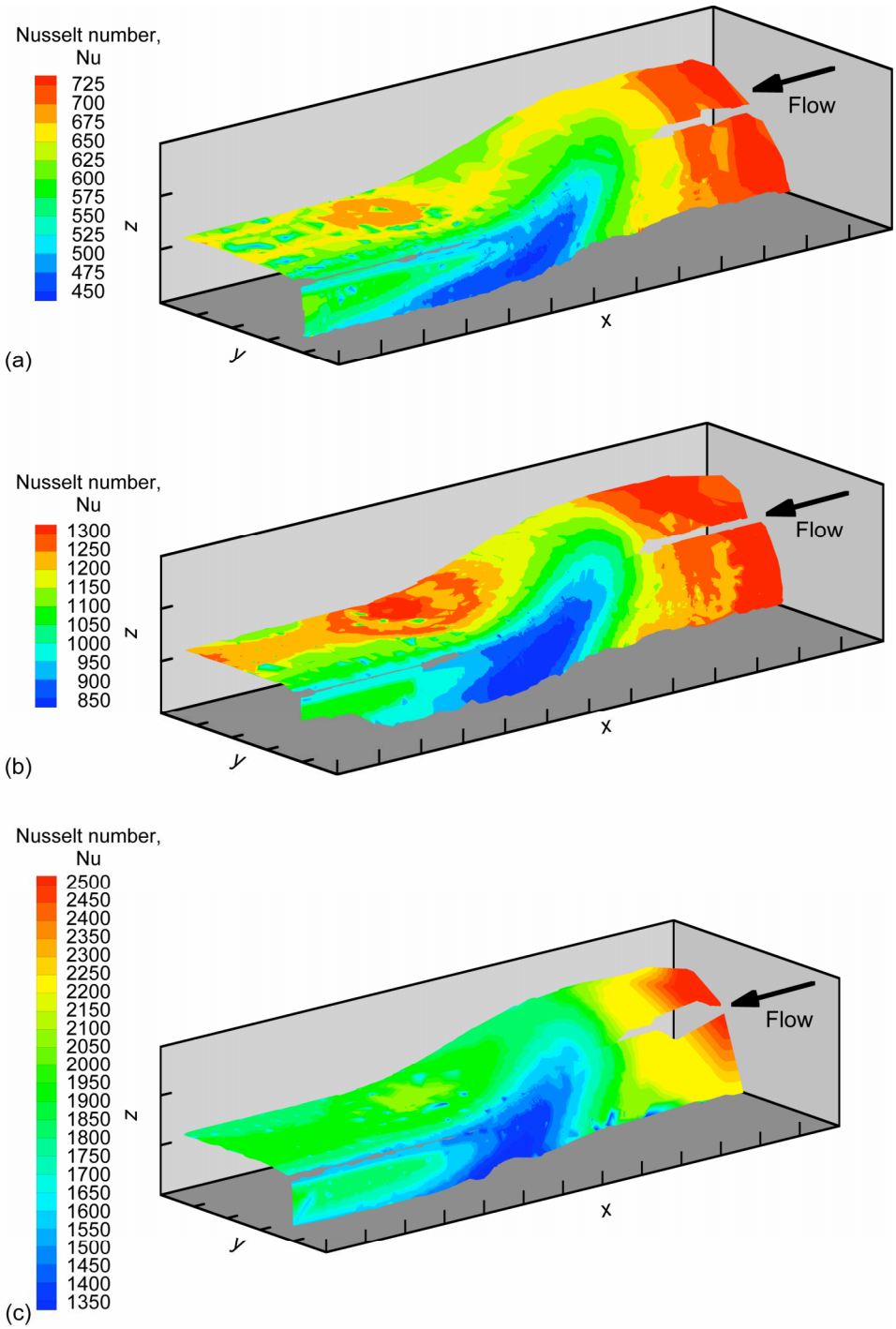

Figure 9.—Heat transfer contours at nominal 16 percent turbulence intensity (*Tu*) at three Reynolds numbers (Re) and Mach numbers (M). (a) Re = 0.4×10^6 and M = 0.08. (b) Re = 0.77×10^6 and M = 0.16. (c) Re = 1.4×10^6 and M = 0.49.

The higher turbulence apparently has reduced the effect of the decreasing pressure gradient on the expanding sidewalls. Comparison of figures 8(a) and 9(a) show that the minimum Nusselt values have increased with turbulence (from 260 to 440) whereas the local maximum seems to have changed much less (from 690 to 740). A curve fit of the data showed that, for the 16-percent-turbulence case, the Nusselt number increased with Reynolds number raised to the 0.9 power.

Figures 10 and 11 show Nusselt numbers normalized by a baseline-calculated Nusselt number for a constant-cross-section round pipe. For the low-turbulence cases at all Reynolds numbers, the heat transfer roughly matches the

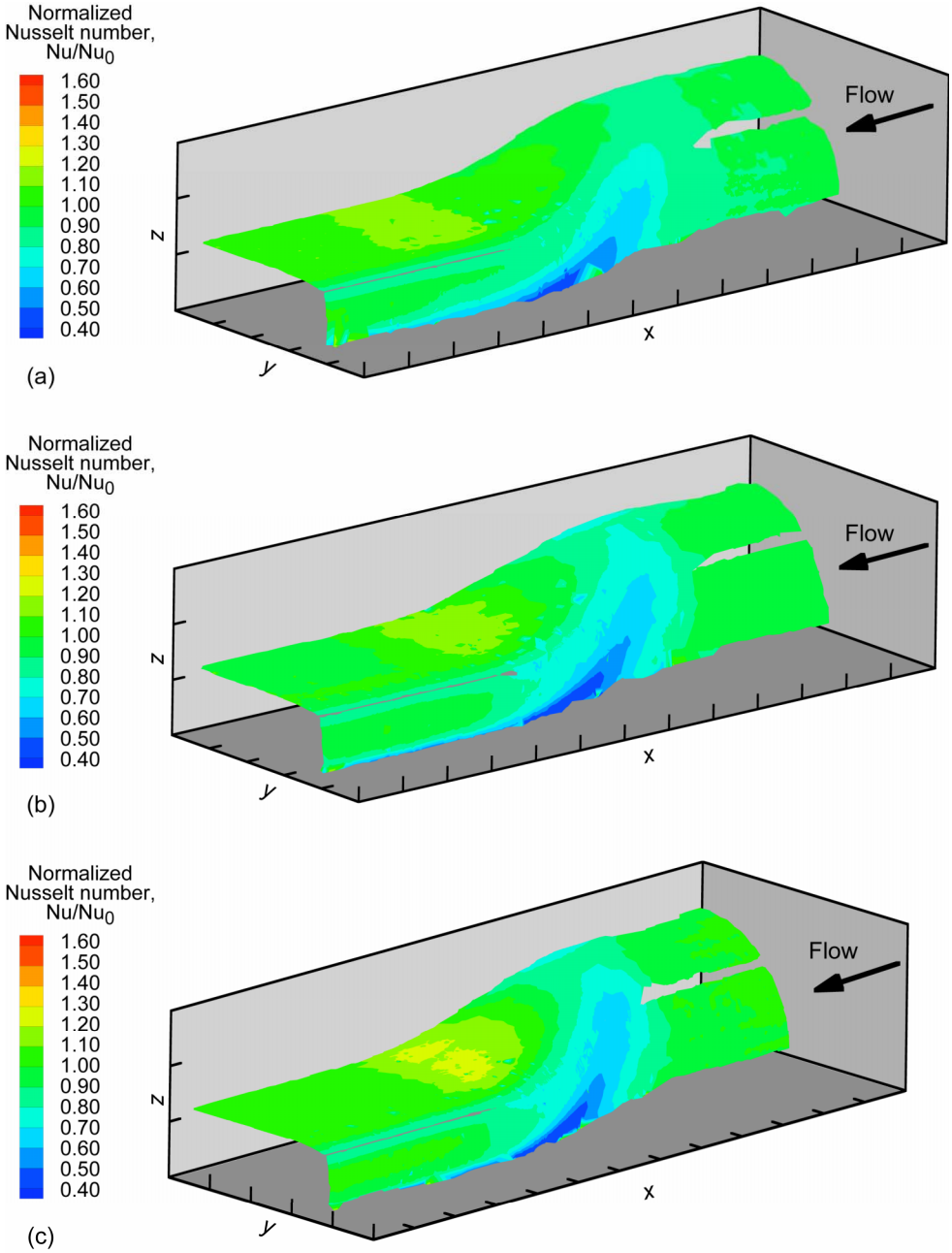

Figure 10.—Normalized heat transfer contours at nominal 1 percent turbulence intensity (*Tu*) at three Reynolds numbers (Re) and Mach numbers (M) where Nu_0 values are Nusselt numbers for turbulent flow in a circular tube. (a) Re = 0.4×10^6 and M = 0.08. (b) Re = 1.6×10^6 and M = 0.34. (c) Re = 2.4×10^6 and M = 0.55.

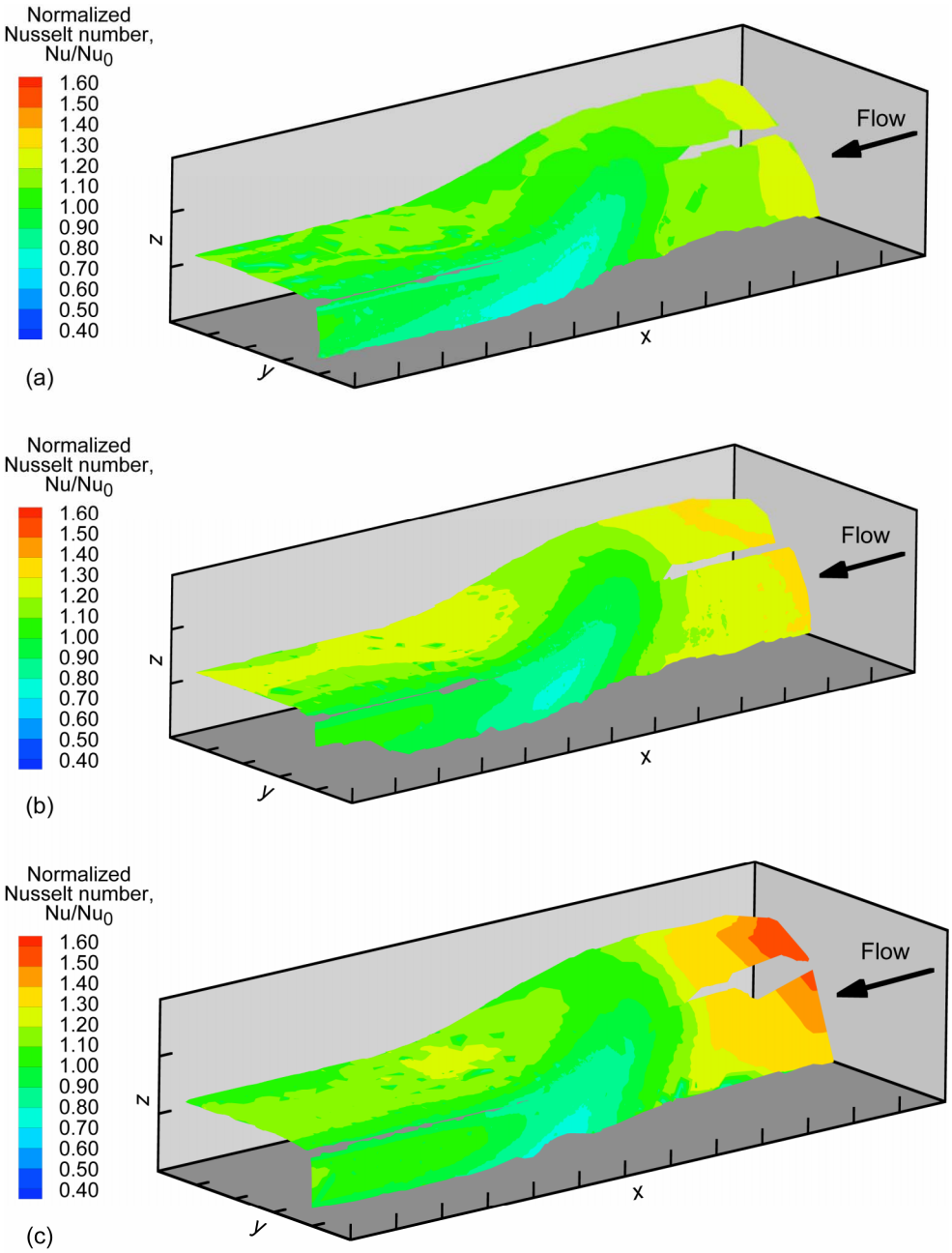

Figure 11.—Normalized heat transfer contours at nominal 16 percent turbulence intensity (*Tu*) at three Reynolds numbers (Re) and Mach numbers (M) where Nu_0 values are Nusselt numbers for turbulent flow in a circular tube. (a) Re = 0.4×10^6 and M = 0.08. (b) Re = 0.77×10^6 and M = 0.34. (c) Re = 1.4×10^6 and M = 0.55.

calculated baseline values in the round inlet section of the duct. As the top of the duct converges, the heat transfer rises above the baseline value. On the sides of the duct where the cross section diverges, heat transfer reaches a minimum level below the straight duct baseline value. For the high-turbulence cases, the heat transfer exhibits similar behavior to the low turbulence cases except near the duct inlet. In this region the higher turbulence dramatically enhances the heat transfer, from 1.2 to 1.5 times the baseline value depending on the Reynolds number.

Concluding Remarks

The transient liquid crystal technique detailed in this paper has proven very effective in obtaining detailed heat transfer maps of test models with compound curved surfaces. This

method, implemented in the NASA Glenn Engine Research Building SW–2 Transition Duct Heat Transfer Tunnel, was used to obtain heat transfer maps of a round-to-rectangular transition duct.

The superelliptic duct surface heat transfer pattern was fairly smooth. The heat transfer was generally highest at the impingement area where top and bottom walls of the duct converge. Nusselt number values at this local maximum increased to values above the straight pipe correlation. Minimum values of heat transfer were observed on the sidewalls where the flow diverges. The Nusselt number decreased to values less than the straight-pipe correlation.

Inlet velocity profiles indicated the flow to be turbulent. Nusselt numbers on the duct surface increased with Reynolds number roughly as expected for turbulent flow conditions.

Higher turbulence intensity increased the heat transfer as expected. Higher turbulence also slightly increased the Reynolds number dependence on Nusselt but generally lessened the range of maximum to minimum heat transfer at a particular Reynolds number.

Appendix A

Symbols

a	geometry coefficient
B	additive constant for law of wall
b	geometry coefficient
c	specific heat at constant pressure
D	duct inlet diameter
H	shape factor
h	heat transfer coefficient
K	factor relating uncertainty in nondimensional temperature to nondimensional time
k_a	thermal conductivity of air
k_w	thermal conductivity of duct wall
M	Mach number
n	geometry exponent
Nu	Nusselt number
Nu_0	Nusselt number for turbulent flow in a circular pipe
Pr	Prandtl number, $c\mu/k_a$
q	heat flux
R	radius
r	recovery factor for turbulent flow, $Pr^{1/3}$
Re	Reynolds number based on duct inlet diameter
s	distance into test surface wall
T	temperature
T_i	initial temperature (duct wall)
T_{lc}	liquid crystal temperature
T_r	recovery temperature (air)
T_s	surface temperature (duct wall)
T_{st}	static temperature (air)
T_{to}	total temperature (air)
Tu	freestream turbulence intensity
t	time
u^+	law of wall velocity
V	duct inlet velocity
V_{max}	maximum velocity
x	duct coordinate, streamwise
y	duct coordinate
y^+	law of wall distance
z	duct coordinate
α	thermal diffusivity, $k_w/(\rho c)$
β	nondimensional time, $ht^{1/2}/(\rho c k_w)^{1/2}$
$\delta_{.95}$	boundary layer thickness
δ^*	displacement thickness
κ	von Karman constant for law of wall
μ	viscosity
ρ	density
θ	nondimensional temperature, $(T_i - T_s)/(T_i - T_r)$
θ_m	momentum thickness

Appendix B

Uncertainty Analysis

Uncertainty calculations were based on methods of Kline and McClintock (ref. 14). The uncertainty in the heat transfer coefficient h was calculated in every different grid square on the duct surface along each isotherm, but only the maximum value along each isothermal line was used. The uncertainty in θ (Δθ) is determined from its defining equation (eq. (4)):

$$\Delta\theta = \sqrt{\left(\left[\frac{1}{T_i - T_r} - \frac{T_i - T_s}{(T_i - T_r)^2}\right]\Delta T_i\right)^2 + \left(\frac{1}{T_r - T_i}\Delta T_s\right)^2 + \left(\frac{T_i - T_s}{(T_i - T_r)^2}\Delta T_r\right)^2} \tag{9}$$

The uncertainty in β (Δβ divided by the value β) is found from the following expression, which relates the uncertainty in β and θ and comes from the error function relationship:

$$K = \frac{\frac{\Delta\beta}{\beta}}{\frac{\Delta\theta}{\theta}} = 0.0006838\beta^4 - 0.018\beta^3 + 0.1742\beta^2 + 0.9722\beta + 0.9917 \tag{10}$$

The root-sum-square uncertainty in h is then calculated from

$$\Delta h = \sqrt{\left(\left[\frac{\sqrt{\rho c k_w}}{\sqrt{t}}\right]\Delta\beta\right)^2 + \left(\frac{-\beta\sqrt{\rho c k_w}}{2\sqrt{t^3}}\Delta t\right)^2 + \left(\frac{\beta}{\sqrt{t}}\Delta\sqrt{\rho c k_w}\right)^2} \tag{11}$$

The uncertainty analysis included the following measurement uncertainties:

ΔT_i, initial duct-surface temperature uncertainty: up to ±0.39 °C (±0.7 °F)

ΔT_s, liquid-crystal calibrated-color temperature uncertainty: ±0.06 °C (±0.1 °F)

ΔT_r, air recovery temperature uncertainty (from the integrated average T_{to} and T_{st} based on the inlet velocity as determined by the pressure measurements): ±0.28 °C (±0.5 °F)

Δt, video-frame time plus start-up time uncertainty: ±0.2 s

$\Delta(\rho c k_w)^{1/2}$, wall thermal properties uncertainty: ±4 percent

Video-frame isotherm-position uncertainty on the models: ±2.5 mm (±0.1 in.), typically

Position uncertainty of grid points on the models: ±1.3 mm (±0.05 in.), typically

The major contributors to the uncertainty in the heat transfer coefficient were ΔT_r, K, and in cases with low initial temperature, ΔT_i. The uncertainty in h (eq. (11)) was nominally ±5 percent.

References

1. Davis, David O.: Experimental Investigation of Turbulent Flow Through a Circular-to-Rectangular Transition Duct. NASA TM–105210, 1991.
2. Reichert, Bruce A.: A Study of High Speed Flows in an Aircraft Transition Duct. NASA TM–104449, 1991.
3. Reichert, B.A.; Hingst, W.R.; and Okiishi, T.H.: An Experimental Comparison of Nonswirling and Swirling Flow in a Circular-to-Rectangular Transition Duct. NASA TM–104359, 1991.
4. Cavicchi, Richard H.: Application of the RNS3D Code to a Circular-Rectangular Transition Duct With and Without Inlet Swirl and Comparison With Experiments. NASA/TM—1999-209394, 1999.
5. Harloff, G.J., et al.: Navier-Stokes Analysis and Experimental Data Comparison of Compressible Flow Within Ducts. NASA TM–105796, 1992.
6. Sotiropoulos, F.; and Patel, V.: Numerical Calculation of Turbulent Flow Through a Circular-to-Rectangular Transition Duct Using Advanced Turbulence Closures. AIAA–93–3030, 1993.
7. Wang, C.R., et al.: Heat Transfer Computations of Internal Duct Flows With Combined Hydraulic and Thermal Developing Length. NASA TM–107450 (AIAA–97–2486), 1997.
8. Hippensteele, Steven A.; and Poinsatte, Philip E.: Transient Liquid-Crystal Technique Used to Produce High-Resolution Convective Heat-Transfer-Coefficient Maps. NASA TM–106083, 1993.
9. Carslaw, H.S.; and Jaeger, J.C.: Conduction of Heat in Solids. Second ed., Oxford University Press, London, 1959.
10. Jones, Terry V.; and Hippensteele, Steven A.: High-Resolution Heat-Transfer-Coefficient Maps Applicable to Compound-Curve Surfaces Using Liquid Crystals in a Transient Wind Tunnel. Developments in Experimental Techniques in Heat Transfer and Combustion (NASA TM–89855), vol. 71, 1987, pp. 1–9.
11. Camci, C.; Kim, K.; and Hippensteele, S.A.: A New Hue Capturing Technique for the Quantitative Interpretation of Liquid-Crystal Images Used in Convective Heat-Transfer Studies. Trans. ASME J. Turbomachinery, ASME Paper 91–GT–122, vol. 114, no. 4, 1992, pp. 765–775.
12. Camci, C., et al.: Evaluation of a Hue Capturing Based Transient Liquid-Crystal Method for High-Resolution Mapping of Convective Heat-Transfer on Curved Surfaces. J. Heat Transfer Trans. ASME, vol. 115, no. 2, 1993, pp. 311–318.
13. Baines, W.D.; and Peterson, E.G.: An Investigation of Flow Through Screens. Trans. ASME, 1951, pp. 467–480.
14. Kline, S.J.; and McClintock, F.A.: Describing Uncertainties in Single-Sample Experiments. Mech. Eng., vol. 75, 1953, pp. 3–7.

Glenn Research Center
National Aeronautics and Space Administration
Cleveland, Ohio, March 25, 2008

REPORT DOCUMENTATION PAGE			Form Approved OMB No. 0704-0188

1. REPORT DATE *(DD-MM-YYYY)*	2. REPORT TYPE	3. DATES COVERED *(From - To)*
01-05-2008	Technical Paper	

4. TITLE AND SUBTITLE
Heat Transfer in a Superelliptic Transition Duct

5a. CONTRACT NUMBER

5b. GRANT NUMBER

5c. PROGRAM ELEMENT NUMBER

6. AUTHOR(S)
Poinsatte, Philip; Thurman, Douglas; Hippensteele, Steven

5d. PROJECT NUMBER

5e. TASK NUMBER

5f. WORK UNIT NUMBER
WBS 561581.02.08.03.02.02

7. PERFORMING ORGANIZATION NAME(S) AND ADDRESS(ES)
National Aeronautics and Space Administration
John H. Glenn Research Center at Lewis Field
Cleveland, Ohio 44135-3191

8. PERFORMING ORGANIZATION REPORT NUMBER
E-16175

9. SPONSORING/MONITORING AGENCY NAME(S) AND ADDRESS(ES)
National Aeronautics and Space Administration
Washington, DC 20546-0001
and
U.S. Army Research Laboratory
Adelphi, Maryland 20783-1145

10. SPONSORING/MONITORS ACRONYM(S)
NASA; ARL

11. SPONSORING/MONITORING REPORT NUMBER
NASA/TP-2008-214943; ARL-TR-4200

12. DISTRIBUTION/AVAILABILITY STATEMENT
Unclassified-Unlimited
Subject Category: 34
Available electronically at http://gltrs.grc.nasa.gov
This publication is available from the NASA Center for AeroSpace Information, 301-621-0390

13. SUPPLEMENTARY NOTES
Heat transfer data for low-turbulence cases are found at http://gltrs.grc.nasa.gov/reports/2008/TP-2008-214943/SE-Nu-lowTu.xls and heat transfer data for high-turbulence cases are found at http://gltrs.grc.nasa.gov/reports/2008/TP-2008-214943/SE-Nu-highTu.xls .

14. ABSTRACT
Local heat transfer measurements were experimentally mapped using a transient liquid-crystal heat transfer technique on the surface of a circular-to-rectangular transition duct. The transition duct had a length-to-diameter ratio of 1.5 and an exit-plane aspect ratio of 3. The cross-sectional geometry was defined by the equation of a superellipse. The cross-sectional area was the same at the inlet and exit but varied up to 15 percent higher through the transition. The duct was preheated to a uniform temperature (nominally 64 °C) before allowing room temperature air to be suddenly drawn through it. As the surface cooled, the resulting isothermal contours on the duct surface were revealed using a surface coating of thermochromic liquid crystals that display distinctive colors at particular temperatures. A video record was made of the surface temperature and time data for all points on the duct surfaces during each test. Using this surface temperature-time data together with the temperature of the air flowing through the model and the initial temperature of the model wall, the heat transfer coefficient was calculated by employing the classic one-dimensional, semi-infinite wall heat transfer conduction model. Test results are reported for inlet diameter-based Reynolds numbers ranging from 0.4×10^6 to 2.4×10^6 and two grid-generated freestream turbulence intensities of about 1 percent, which is typical of wind tunnels, and up to 16 percent, which may be more typical of real engine conditions.

15. SUBJECT TERMS
Heat transfer; Transition duct; Liquid crystal; Heat transfer coefficient

16. SECURITY CLASSIFICATION OF:			17. LIMITATION OF ABSTRACT	18. NUMBER OF PAGES	19a. NAME OF RESPONSIBLE PERSON
a. REPORT	b. ABSTRACT	c. THIS PAGE			STI Help Desk (email:help@sti.nasa.gov)
U	U	U	UU	22	19b. TELEPHONE NUMBER *(include area code)* 301-621-0390